2023 IEEE International Conference on Robotics and Automation (ICRA 2023)
May 29 - June 2, 2023. London, UK

A Non-planar Assembly of Modular Tetrahedral-shaped Aerial Robots

Obadah Wali, Mohamad T. Shahab, and Eric Feron

***Abstract*— This paper presents a new design of aerial vehicles with tetrahedral geometry. We call this design the TetraQuad. The TetraQuad is a fractal modular aerial robot. A characteristic of fractals is that they have a geometric shape that can be assembled to generate the same geometry on a larger scale. Therefore multiple TetraQuad modules can be assembled to produce a larger scaled tetrahedral shaped aerial vehicle. The advantage is to have modular aerial robots that assemble in the vertical direction; this increases the rigidity of the structure, as well as reduces the wake interaction of the elevated propellers in the assembly. This work presents a design and analysis of the TetraQuad module as well as assemblies of multiple modules. A modular controller strategy is discussed. The functionality of the controller is illustrated using simulations. We validate our design with experimental flight tests.**

I. Introduction

The design of multiple robots assembled systems is of interest in robotics fields, in particular modular robot systems [1]. Multiple studies have investigated the design of modular ground and underwater robots for different purposes as in [16], [12], [2], [23], [3], and [13]. In addition, this interest extends to modular aerial robots.

There are many designs of modular aerial robots. In [5] the authors explore a design of multi modular vertical take-off and landing, or VTOL, aerial vehicles. Other works are more focused on the multiple multirotor unmanned aerial vehicles, or UAV's. In [17], the authors designed a hexagon shaped planar robot with a single rotor with the aim to self-assemble in the ground to the needed shape before flying as an assembled unit. In [11], two dual-rotor modules are connected to achieve a high degree of maneuverability. In [24], the authors introduce a transformable aerial robot which is a composite of dual-rotor modules, with the goal of having flexible joining and maneuvering. The design in [14] proposes modular rotors for the goal of flying rigid objects. Another work is [15] where the authors used modular ducted-fan vehicles to achieve the flying of connected modular vehicles. In all of the aerial robots above, except the one from [5], individual modules in the assembly system are not able to fly on their own; hence, adaptability while flying is limited.

There exists more complicated systems consisting of multiple multirotor modules, where each module can fly alone and in assembly. For example, in [6] quadrotor modules are assembled together to increase the lifting payload. Another project that utilized quadrotors is [19] and [22], where planar in-air assembly of multiple quadrotors is achieved. In addition in [20] a self-disassembly during flight is executed. However, the above designs have only planar connection between the modules and are not vertically connected. In [9] vertically assembled fractal aerial robots are discussed where single-rotor modules can assemble both horizontally and vertically, although modules are not able to fly alone.

The authors are with the Robotics, Intelligent Systems, and Control (RISC) Lab, King Abdullah University of Science and Technology (KAUST), Thuwal 23955, Saudi Arabia. Emails: {obadah.wali,mohamad.shahab,eric.feron}@kaust.edu.sa.

Support for the work was provided by KAUST faculty baseline fund.

The authors would like to acknowledge the help of Bilal Maassarani and Kuat Telegenov.

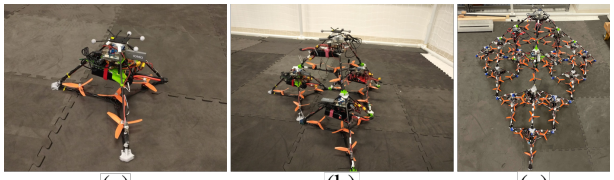

Fig. 1. (a) one TetraQuad module; (b) the four-TetraQuad assembly (c) the sixteen-TetraQuad assembly

The work in [10], by a co-author of the present paper, lays a foundation for the study of fractal tetrahedral shaped quadrotors. A characteristic of fractals is that they have a geometric shape that can be assembled to generate the same geometry on a larger scale. This design serves two main objectives. First, we want to have an assembly which enhances structural rigidity during flight. Second is to reduce the wake interaction between rotors in the multi-plane assembly; see [7]. However, flight of assembled fractal tetrahedral shaped modules was not presented before.

In this present paper a new design of the tetrahedral shaped flying robot is introduced, which we call the TetraQuad. The contributions of this paper are as follows. As the main contribution, we present a new design of a tetrahedral shaped flying module. We also show that we are able to assemble multiple modules and fly a larger tetrahedral shaped system, and with a modular control strategy. We validate our system by conducting multiple experimental flying tests. As far as the authors are aware, systems of multiple vertically-assembled multi-rotor modules have not been validated before.

II. Single and Assembled Modules of TetraQuad

The TetraQuad is a tetrahedron shaped vehicle with equilateral triangle facets. The dihedral angle between the bottom facet and other facets is 45 degrees. The tetrahedron dimensions are 430 mm long, 370 mm width, and 260 mm height. The tilted edges of this frame are made of carbon fiber tubes with a 5mm diameter. The bottom facet's chassis is made of 4mm thick carbon fiber plates. All joints of the structure are 3D-printed using a PLA with 0.15 layers and 80% filling. See Figure 2.

Actuation of one module of the TetraQuad consists of four 5-inch propellers which actuate using brushless motors. The propellers are located on the bottom facet of the tetrahedron. One propeller is positioned at the center of the facet. The

other three are located at the three lines that connect the vertices of the bottom facet to its center. The distance between each of the three lateral propellers and the middle one is $d = 103$ mm. All electronics, including a flight controller, an on-board computer, and power electronics are located on a plate, which is located at the upper half of the vehicle structure. Each module is equipped with one 4-cell Lipo battery of 3700 mA capacity. The total weight of one module is 890g. These components are illustrated in Figure 2.

The modules assemble by connecting their tetrahedron vertices together; see Figure 1. In a four-module assembly, the top module base vertices are connected to the top vertices of the three bottom modules. Besides, the bottom front module rear vertices are connected to the front vertices of the rear bottom modules. Similarly, the right bottom module is jointed to the left vertices of the other bottom modules, while the left module is attached to the right vertices of the other bottom modules. This connection structure extends to assemblies of four modules to generate an assembly of sixteen modules, and so forth.

For an assembly of N modules, all modules are identical. Each module, $i \in \{1, 2, \ldots, N\}$, generates its moments $\mathbf{M}_i \in \mathbb{R}^3$ and thrust T_i by changing the moment and thrust of its four propellers $\tau_{i,j}$ and $F_{i,j}$, $(j \in \{1, 2, 3, 4\})$, respectively. Define the normal vector $\mathsf{e}_3 := \begin{bmatrix} 0 & 0 & 1 \end{bmatrix}^\top \in \mathbb{R}^3$. Then the moments and thrusts are given by

$$\mathbf{M}_i = \sum_{j=1}^{4} \mathbf{r}_j \times \mathsf{e}_3 F_{i,j} + \mathsf{e}_3 \tau_{i,j},$$

$$T_i = \sum_{j=1}^{4} F_{i,j},$$

where $\mathbf{r}_j$ is the position of rotor j relative to the module's center of mass, namely $\mathbf{r}_1 = [0\ 0\ 0]^\top$, $\mathbf{r}_2 = [d\ 0\ 0]^\top$, $\mathbf{r}_3 = [-\frac{1}{2}d\ \frac{\sqrt{3}}{2}d\ 0]^\top$, and $\mathbf{r}_4 = [-\frac{1}{2}d\ -\frac{\sqrt{3}}{2}d\ 0]^\top$; indeed $\tau_{i,j}$ and $F_{i,j}$ are changed by changing the angular velocities $\omega_{j,i}$ of the corresponding propeller through the relations $\tau_{i,j} = k_M \omega_{j,i}^2$ for $j = 1, 4$ (counterclockwise), $\tau_{i,j} = -k_M \omega_{j,i}^2$ for $j = 2, 3$ (clockwise), $F_{i,j} = k_T \omega_{j,i}^2$ for every j, with k_T as the rotor thrust constant, k_M as the rotor drag constant. Notice that the relationship between a module's generated moments and thrust and its propellers' angular velocities is one-to-one, justifying using $\mathbf{M}_i, T_i$ directly as the control input of module i. In particular, we have

$$\begin{bmatrix} T_i \\ \mathbf{M}_i \end{bmatrix} = \begin{bmatrix} k_T & k_T & k_T & k_T \\ 0 & 0 & dk_T\sqrt{3}/2 & -dk_T\sqrt{3}/2 \\ 0 & dk_T & -dk_T/2 & -dk_T/2 \\ k_M & -k_M & -k_M & k_M \end{bmatrix} \begin{bmatrix} \omega_{1,i}^2 \\ \omega_{2,i}^2 \\ \omega_{3,i}^2 \\ \omega_{4,i}^2 \end{bmatrix}. \tag{1}$$

In practice, each propellers' moment and thrust are bounded, namely $0 \le F_{i,j} \le F_{\max}$, $0 \le \tau_{i,j} \le \tau_{\max}$ for $j = 1, 4$ (counterclockwise) and $-\tau_{\max} \le \tau_{i,j} \le 0$ for $j = 2, 3$ (clockwise). You can find these bounds for our system in Table II. For more analysis about thrust limits related to tetrahedral assemblies of vehicles, see [21].

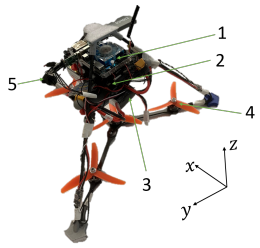

Fig. 2. A TetrQuad module; (1) On-board computer: ODROID with a Wi-Fi module, (2) flight controller, (3) battery, (4) 5-inch propeller and brushless motor, and (5) front vertex of the tetrahedron.

TABLE I

SYSTEM PARAMETERS

m_0 (kg)	L (m)	$I_{xx,0}$ (kg · m^2)	$I_{yy,0}$ (kg · m^2)	$I_{zz,0}$ (kg · m^2)
0.89	0.355	7.5×10^{-3}	7.5×10^{-3}	6.8×10^{-3}

TABLE II

SYSTEM SPECIFICATIONS

F_{max} (N)	τ_{max} (N · m)
5.3	0.78

III. THE TETRAHEDRON ASSEMBLY MOMENT OF INERTIA

We now present the system inertia, which is changing as the number of modules in the assembly increases. Let $I_0 \in \mathbb{R}^{3\times3}$ be the inertia matrix associated with the individual tetrahedral shaped module. We assume that its principle axes are such that $I_0 = \mathrm{diag}(I_{xx,0}, I_{yy,0}, I_{zz,0})$. Let $I_n = \mathrm{diag}(I_{xx,n}, I_{yy,n}, I_{zz,n}) \in \mathbb{R}^{3\times3}$ be the inertia matrix associated with the whole assembly of $N = 4^n$ modules; in our case, because of the tetrahedral shape it is possible to have an assembly of 4^n modules, $n = 0, 1, 2, \ldots$ and so on. In the following we are going to analyze the tetrahedron assembly in detail and calculate I_n when $n \neq 0$. In our calculation of moment of inertia of a larger assembly we assume that the module is a uniform tetrahedron. We also consider that modules are connected together rigidly, and that modules' frames are parallel to the assembly body frame. For four modules the calculation of the new moment of inertia components requires defining the following quantities: m_0 as the mass of an individual module, L as the edge length of each individual module, H as the height of the individual module, and l as the third of the vehicle length in x-direction; see Figure 3. These quantities are related:

$$H = \frac{\sqrt{3}}{2}L, \tag{2}$$

$$l = \frac{\sqrt{3}L}{6}. \tag{3}$$

Figure 3(a) indicates the rotation about the x-axis of four assembled modules. Thus using the parallel axis theorem and the relation in (2) we can find the new center of mass in relation to one module center of mass and obtain

$$I_{xx,1} = 4I_{xx,0} + \frac{13}{12}L^2 m_0. \tag{4}$$

Similarly the moment of inertia about z-axis of four assem-

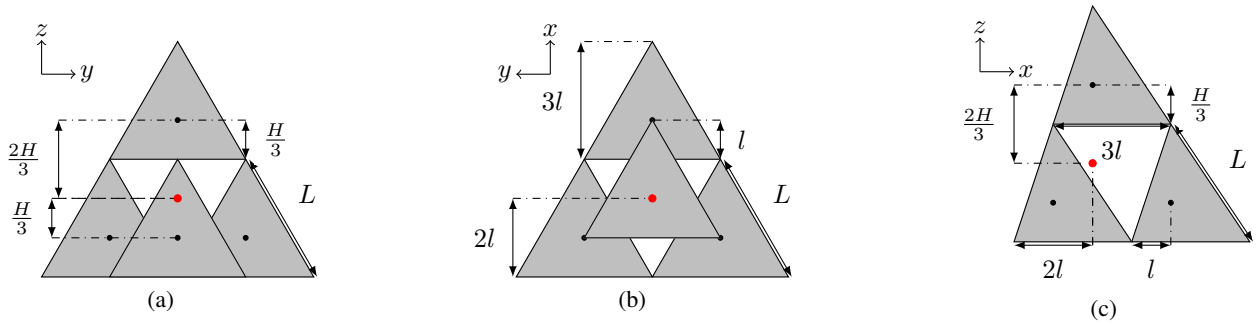

Fig. 3. Four-tetrahedron assembly 2D drawing views (a) Front view. The axis of rotation is the x-axis (red dot), (b) Top view. The axis of rotation is the z-axis (red dot), and (c) side view. The axis of rotation is the y-axis (red dot). Black dots represent the center of mass of each module.

bled modules, as represented in Figure 3(b), can be calculated utilizing (3) to obtain

$$I_{zz,1} = 4I_{zz,0} + L^2 m_0. \tag{5}$$

In a similar fashion, referring to Figure 3(c), the moment of inertia about y-axis relation can be formulated as

$$I_{yy,1} = 4I_{yy,0} + \frac{13}{12}L^2 m_0. \tag{6}$$

1) General formula of the inertia components: By induction, a generalized formula of the inertia elements depending on the number of assembled modules 4^n is obtained in a recursive manner. For $n = 1, 2, 3, \ldots$, we have

$$I_{xx,n} = 4I_{xx,n-1} + \tfrac{13}{12}(16^{n-1})L^2 m_0, \tag{7}$$

$$I_{yy,n} = 4I_{yy,n-1} + \tfrac{13}{12}(16^{n-1})L^2 m_0, \tag{8}$$

$$I_{zz,n} = 4I_{zz,n-1} + 16^{n-1}L^2 m_0. \tag{9}$$

IV. The Controller and its Analysis

In this section, we discuss the control of the tetrahedron assembly. We control thrust and moments of the whole assembled body indirectly; indeed, we control the assembly through the respective actuators of identical TetraQuad modules, i.e. through each module's four propellers. Irrespective of modules' locations in the assembly structure, they all have the same flight controller. This design emphasizes the modularity of the system; however the modules are assembled together, we show that the whole system would fly as desired, presenting a good deal of adaptability. In the following we discuss the attitude controller and the altitude controller of each module, and we analyze them.

We adopt an off-the-shelf attitude and altitude controllers for quadrotors, and show how they are applied, in a distributed manner, to the rigid assembly of tetrahedral quadrotor modules. The attitude and the altitude controllers of each individual TetraQuad module utilizes those of the widely-used PX4 Autopilot[1] [18], where the attitude controller itself is based on the one of [4].

In order to analyze our proposed control strategy, before presenting the details of the controllers we discuss the dynamic model of our system.

[1]https://github.com/PX4/PX4-Autopilot (v1.13)

A. System dynamics

Here we discuss the attitude dynamics and altitude dynamics. Because the attitude controller we apply (which is going to be discussed shortly) uses quaternion representation, then it is appropriate if the dynamics of the system are also written using quaternion representation. To this end, the attitude dynamics can be written as follows [8]:

$$\dot{\mathbf{Q}} = -\frac{1}{2}\begin{bmatrix}0\\ \boldsymbol{\Omega}\end{bmatrix} \otimes \mathbf{Q} \tag{10}$$

where $\mathbf{Q} = [Q_0 \;\; Q_1 \;\; Q_2 \;\; Q_3]^\top \in \mathbb{R}^4$ is the quaternion representation of orientation of the whole rigid assembly, and $\boldsymbol{\Omega}$ in $\mathbb{R}^3$ is the corresponding angular velocity vector in the assembly body frame; the operation $\otimes$ is the quaternion product: for $\mathbf{Q}, \mathbf{P} \in \mathbb{R}^4$ with $\mathbf{Q} = [Q_0 \;\; \bar{\mathbf{Q}}^\top]^\top$, $\bar{\mathbf{Q}} = [Q_1 \;\; Q_2 \;\; Q_3]^\top$, $\mathbf{P} = [P_0 \;\; \bar{\mathbf{P}}^\top]^\top$ and $\bar{\mathbf{P}} = [P_1 \;\; P_2 \;\; P_3]^\top$, then

$$\mathbf{Q} \otimes \mathbf{P} = \begin{bmatrix} Q_0 P_0 - \bar{\mathbf{Q}} \cdot \bar{\mathbf{P}} \\ P_0 \bar{\mathbf{Q}} + Q_0 \bar{\mathbf{P}} + \bar{\mathbf{Q}} \times \bar{\mathbf{P}} \end{bmatrix}.$$

With $\boldsymbol{\Omega} = \begin{bmatrix} p & q & r \end{bmatrix}^\top \in \mathbb{R}^3$, then, by defining $\mathbf{M} := \begin{bmatrix} M_x & M_y & M_z \end{bmatrix}^\top \in \mathbb{R}^3$ with M_x, M_y and M_z denoting the total applied roll, pitch, and yaw moments, respectively, the angular dynamics can be represented by

$$I\dot{\boldsymbol{\Omega}} = -\boldsymbol{\Omega} \times [I\boldsymbol{\Omega}] + \mathbf{M}, \tag{11}$$

with I as the moment of inertia of the whole assembly system, i.e. $I = I_n$.

We now provide the altitude dynamics. We have a world frame defined by x, y and z axes, with the z-axis pointing upward. We consider that the center of mass of the assembly is situated at the origin of a body frame. Let $\mathbf{p} = [x \; y \; z]^\top \in \mathbb{R}^3$ be the coordinates of the center of mass of the whole assembly in the world frame, with z indicating the altitude. We have $R \in \mathbb{R}^{3\times 3}$ as the rotation matrix transforming coordinates from the assembly body frame to the world frame; then let R_{33} denote the element in R in the third column and the third row. With T denoting the total thrust produced by the assembly of modules, the altitude dynamics can be represented by

$$m\ddot{z} = -mg + R_{33}T \tag{12}$$

with m and g denoting the mass of the whole assembly and the gravitational acceleration, respectively.

As we control the system indirectly through the TetraQuad modules, we present now how the forces and moments

applied onto the assembly are generated. For each $i \in \{1, 2, \ldots, N\}$, we have T_i and $\mathbf{M}_i = \begin{bmatrix} M_{i,x} & M_{i,y} & M_{i,z} \end{bmatrix}^\top$ to denote respectively the thrust force and the moments generated by module i with respect to module body frame. As the modules are connected together rigidly, and each module's frame is parallel to the assembly body frame, then we can write the total thrust and moments applied on the whole assembly in a simple manner. Let $\mathbf{p}_i^{\mathcal{B}} = \begin{bmatrix} x_i^{\mathcal{B}} & y_i^{\mathcal{B}} & z_i^{\mathcal{B}} \end{bmatrix}^\top$ be the x-, y and z-coordinates of the center of mass of module i in the whole assembly body frame; then we obtain

$$T = \sum_{i=1}^{N} T_i, \tag{13a}$$

$$\mathbf{M} = \sum_{i=1}^{N} \mathbf{M}_i + \mathbf{p}_i^{\mathcal{B}} \times \mathbf{e}_3 T_i. \tag{13b}$$

This allows modules to be on different planes in the assembly, as a tetrahedron assembly would.

B. The Flight Controller

We now present both the attitude and the altitude controllers.

1) The Attitude Controller: To control the attitude (the orientation) of the assembly, we set control commands for $\mathbf{M}_i$ for all modules. For each module i, the input to attitude controller are the measured quaternion vector $\mathbf{Q}_i$ and the setpoint quaternion vector $\mathbf{Q}_{\text{sp}}$; the output of the attitude controller are the moments command $\mathbf{M}_{i,\text{cmd}}$.

The attitude controller consists of two cascade controllers. One is a nonlinear controller and the second controller is a PID controller. Define the error $\mathbf{e}_i = \mathbf{Q}_i^{-1} \otimes \mathbf{Q}_{\text{sp}}$, with $\mathbf{Q}_i^{-1} = \mathbf{Q}_i^* / \|\mathbf{Q}_i\|$. With $\mathbf{e}_i$ partitioned as $\mathbf{e}_i = [e_{i,0} \ \bar{\mathbf{e}}_i^\top]^\top$, the output of the first controller is the setpoint angular velocity as follows:

$$\mathbf{\Omega}_{i,sp} = K_{P1} sgn(e_{i,0}) \bar{\mathbf{e}}_i, \tag{14}$$

where $sgn(\cdot)$ is the sign function, and $K_{P1} = \text{diag}(K_{P1,x}, K_{P1,y}, K_{P1,z})$ is a gain 3×3 diagonal matrix. The second controller is a PID controller. Define the angular velocity error $\mathbf{e}_{i,\Omega} = \mathbf{\Omega}_{i,sp} - \mathbf{\Omega}_i$, so we can set

$$\mathbf{M}_{i,\text{cmd}} = K_{P2} \mathbf{e}_{i,\Omega} + K_D \dot{\mathbf{e}}_{i,\Omega} + K_I \int \mathbf{e}_{i,\Omega} \, dt \tag{15}$$

with $K_I = \text{diag}(K_{I,x}, K_{I,y}, K_{I,z})$, $K_{P2} = \text{diag}(K_{P2,x}, K_{P2,y}, K_{P2,z})$, and $K_D = \text{diag}(K_{D,x}, K_{D,y}, K_{D,z})$, as 3×3 gain diagonal matrices.

2) The Altitude Controller: The input to the altitude controller is the assembly altitude measurement z, and the setpoint desired altitude z_{sp}. The altitude controller also consists of two cascaded controller. Define the altitude error $e_z = z_{sp} - z$. The output of the first controller is vertical velocity setpoint $\dot{z}_{sp}$ as follows:

$$\dot{z}_{sp} = K_{P1,\text{alt}} e_z \tag{16}$$

where $K_{P1,\text{alt}}$ is a gain. Define the velocity error $e_{vz} = \dot{z}_{sp} - \dot{z}$; the second controller is PID controller and its output is an acceleration command:

$$a_{z,\text{cmd}} = K_{P2,\text{alt}} e_{vz} + K_{D,\text{alt}} \dot{e}_{vz} + K_{I,\text{alt}} \int e_{vz} \, dt \tag{17}$$

with $K_{I,\text{alt}}$, $K_{P2,\text{alt}}$, and $K_{D,\text{alt}}$ as gains. Then, a module i thrust command is set as

$$T_{i,\text{cmd}} = m_0 (g + a_{z,\text{cmd}}) \tag{18}$$

where m_0 is the mass of the individual module.

3) The Total Controller : As mentioned earlier, to retain the modular design of our system we assume that modules' controllers to be identical, irrespective of its location in the assembly. To this end, the applied thrust and moments for each module $i \in \{1, 2, \ldots, N\}$ are set as

$$T_i = T_{i,\text{cmd}}, \tag{19a}$$

$$\mathbf{M}_i = \mathbf{M}_{i,\text{cmd}}. \tag{19b}$$

Next, we analyze the performance of the proposed controller.

C. Analysis of the closed-loop system

Here we analyze the closed-loop system and evaluate its performance. Next, we provide a model for the closed-loop system of the whole tetrahedron assembly; this will give us insight about the closed-loop performance. We consider analyzing the closed-loop system around hovering conditions. In particular, in this analysis we consider $\mathbf{Q}_{\text{sp}} = [1 \ 0 \ 0 \ 0]^\top$ and $\mathbf{\Omega}_{sp} = [0 \ 0 \ 0]^\top$; note that this corresponds to desired orientation of the assembly body in Euler angles representation of $(\phi, \theta, \psi) = (0, 0, 0)$, with the yaw angle ψ about the z-axis, the roll angle ϕ about the x-axis, and the pitch angle θ about the y-axis. Also consider $z_{sp} = z_d$ for some desired constant altitude z_d, so $\dot{e}_z = -\dot{z}$. Also for the simplicity of the analysis, we consider zero values for the derivative term gains in the corresponding PID controllers, namely $K_D = 0$ and $K_{D,\text{alt}} = 0$. Before proceeding, note here that as modules are connected together rigidly, and each module's frame is parallel to the assembly body frame, then $\mathbf{Q}_i = \mathbf{Q}$ for all i. Furthermore, as all module are identical, then $m = N m_0$. Define the states

$$\mathbf{x} = \begin{bmatrix} Q_0 & Q_1 & Q_2 & Q_3 & p & q & r & p_{\text{int}} & q_{\text{int}} & r_{\text{int}} & e_z & \dot{z} & z_{\text{int}} \end{bmatrix}^\top,$$

with $[p_{\text{int}} \ q_{\text{int}} \ r_{\text{int}}]^\top = \int \mathbf{e}_{i,\Omega} \, dt$, and $z_{\text{int}} = \int e_{vz} \, dt$. Then, we combine the system dynamics described by (10), (11), (12) and (13), with the controllers described by (14), (15), (16), (17), (18) and (19), and appropriately define a nonlinear function $f(\cdot)$ such that we obtain

$$\dot{\mathbf{x}} = f(\mathbf{x}). \tag{20}$$

Let $\mathbf{0}_{p \times q}$ denote the matrix of size $p \times q$ whose all of its entries are zero. To analyze the closed-loop behavior around the hovering conditions, then we can linearize (20) about the equilibrium point $\bar{\mathbf{x}} = [1 \ \mathbf{0}_{1 \times 12}]^\top$. If we define $\delta \mathbf{x} = \mathbf{x} - \bar{\mathbf{x}}$, then we can approximate the closed-loop dynamics as follows: $\dot{\delta \mathbf{x}} \approx \left[\frac{\partial}{\partial \mathbf{x}} f(\mathbf{x}) |_{\mathbf{x} = \bar{\mathbf{x}}} \right] \delta \mathbf{x}$.

In our tetrahedron assembly, observe that for every $N = 4^n$, $n = 0, 1, 2, \ldots$, the assembly structure is symmetric about the body x-axis, so we have $\sum_{i=1}^{N} y_i^{\mathcal{B}} = 0$. On the other hand, although the assembly shape is not symmetric about the y-axis, nevertheless a property of tetrahedral as-

sembly of identical tetrahedral modules yields $\sum_{i=1}^{N} x_i^{\mathcal{B}} = 0$ as well. With that, after doing the required calculations the closed-loop dynamics around hovering condition can be written in a decoupled manner. First, we see that $\dot{Q}_0 = 0 \Rightarrow Q_0(t) = 1, t \geq 0$. The corresponding roll, pitch and yaw closed-loop dynamics can be written, respectively, as follows

$$\begin{bmatrix} \dot{Q}_1 \\ \dot{p} \\ \dot{p}_{\text{int}} \end{bmatrix} = \begin{bmatrix} 0 & \frac{1}{2} & 0 \\ -\frac{N(K_{P1,x}+K_{P2,x})}{I_{xx}} & -\frac{NK_{P2,x}}{I_{xx}} & \frac{NK_{I,x}}{I_{xx}} \\ -1 & 0 & 0 \end{bmatrix} \begin{bmatrix} Q_1 \\ p \\ p_{\text{int}} \end{bmatrix} \quad (21)$$

$$\begin{bmatrix} \dot{Q}_2 \\ \dot{q} \\ \dot{q}_{\text{int}} \end{bmatrix} = \begin{bmatrix} 0 & \frac{1}{2} & 0 \\ -\frac{N(K_{P1,y}+K_{P2,y})}{I_{yy}} & -\frac{NK_{P2,y}}{I_{yy}} & \frac{NK_{I,y}}{I_{yy}} \\ -1 & 0 & 0 \end{bmatrix} \begin{bmatrix} Q_2 \\ q \\ q_{\text{int}} \end{bmatrix} \quad (22)$$

$$\begin{bmatrix} \dot{Q}_3 \\ \dot{r} \\ \dot{r}_{\text{int}} \end{bmatrix} = \begin{bmatrix} 0 & \frac{1}{2} & 0 \\ -\frac{N(K_{P1,z}+K_{P2,z})}{I_{zz}} & -\frac{NK_{P2,z}}{I_{zz}} & \frac{NK_{I,z}}{I_{zz}} \\ -1 & 0 & 0 \end{bmatrix} \begin{bmatrix} Q_3 \\ r \\ r_{\text{int}} \end{bmatrix}. \quad (23)$$

Finally, we can describe the altitude closed-loop dynamics by

$$\begin{bmatrix} \dot{e}_z \\ \dot{z} \\ \dot{z}_{\text{int}} \end{bmatrix} = \begin{bmatrix} 0 & -1 & 0 \\ K_{P1,\text{alt}}K_{P2,\text{alt}} & -K_{P2,\text{alt}} & K_{I,\text{alt}} \\ K_{P2,\text{alt}} & -1 & 0 \end{bmatrix} \begin{bmatrix} e_z \\ \dot{z} \\ z_{\text{int}} \end{bmatrix}. \quad (24)$$

The equations (21)–(24) describe the closed-loop dynamics around the hovering conditions which make them applicable to evaluate many applications of our system. We make the following observations.

We can see from (24) that the altitude dynamics are independent of the number of modules in the assembly system; this renders tuning the altitude control performance of the whole assembly to be equivalent to tuning the altitude controller of an individual module. This emphasizes even more the modularity of our design.

For different $N = 4^n, n \in \{0, 1, 2, \ldots\}$, tuning the attitude controller for different assembly structures is dependent on the quantity $\frac{N}{I_{jj}}, (j \in \{x, y, z\})$. In the previous section we have shown how the moment of inertia of the tetrahedron assembly I_{jj} change with respect to the number of modules. The decoupled nature of the system allows us to tune the attitude controller of the identical modules in a simple manner.

Related to the previous point and to understand more the performance of the controller, we provide a root-locus analysis to compare between cases of $n = 0, 1, 2$ in the tetrahedron assembly, i.e. between controlling one, four, and sixteen modules, respectively. We focus on the pitch system in (22); of course similar conclusions can be inferred for the roll and the yaw systems (21) and (23). Refer to Table I for the system parameters; we calculate the moments of inertia for different values of n from Section III. Consider controller gains $K_{P1,y} = 6.5, K_{D,y} = 0, K_{I,y} = 0.2$, and a variable $K_{P2,y} = 0.15k$, for $k \in [0.1, 2.5]$. See the root-locus plot for these range of gains in Figure 4. We see that all poles of the system have negative real parts, i.e. stable. One pole is always real and has value around -0.03. Observe that as the gain $K_{P2,y}$ get larger, the complex poles become real ones and hence the system would have less oscillations; although you can see that for the specified gain range of values, oscillations would not disappear for an assembly of 16 modules; however in all cases, stability of the system is not compromised.

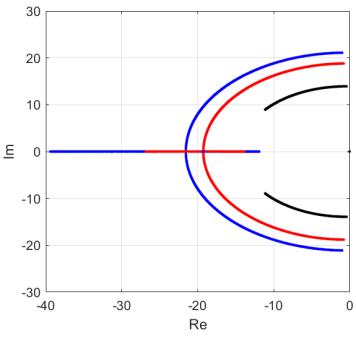

Fig. 4. Root-locus of the pitch system for an assembly of one (blue), four (red) and 16 (black) modules.

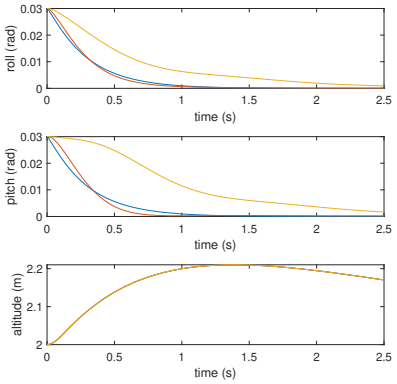

Fig. 5. First simulation example for one (blue), 4 (orange) and 16 (yellow) modules.

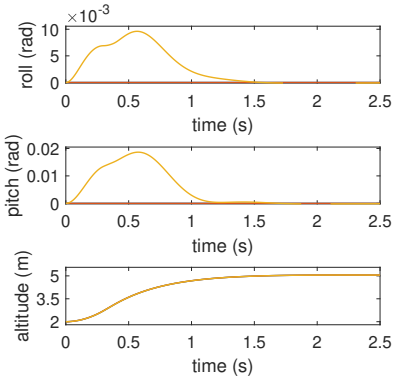

Fig. 6. Second simulation example for one (blue), 4 (orange) and 16 (yellow) modules.

V. Numerical Simulations

Here we provide simulation examples for the system response. We compare the cases when $n = 0, 1, 2$ in the tetrahedron assembly. We consider the system with the parameters in Table I and the system specifications as in Table II. We do the simulation using the SIMULINK model in `https://github.com/mohshahab/Tetra_Simulink`, where we consider the full nonlinear dynamics of the assembly rigid body, including the exerted thrust and moment as in (13); for each module in the assembly, we apply the controller (14)–(18) in a discrete-time manner with sampling time of 0.01s; controller gains are set as to $K_{P1,x} = K_{P1,y} = 6.5, K_{P1,z} = 2.8, K_{P2,x} = K_{P2,y} = K_{P2,z} = 0.15, K_{I,x} = K_{I,y} = K_{I,z} = 0.2, K_{D,x} =$

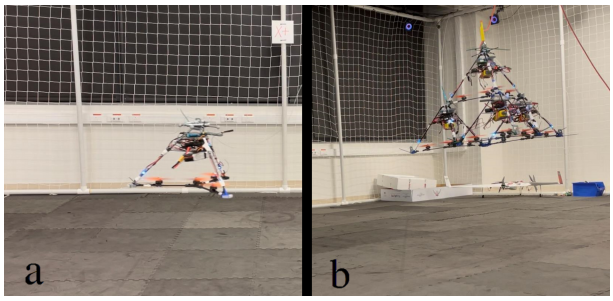

Fig. 7. (a) Flight test of one TetraQuad module; (b) flight test of four assembled TetraQuad modules.

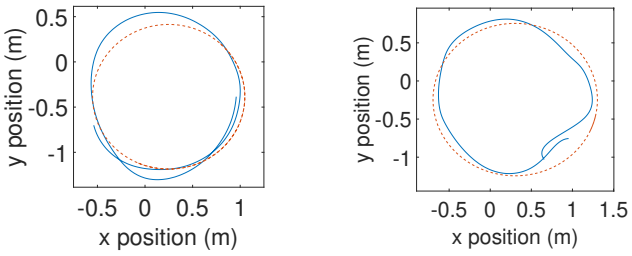

Fig. 8. Circular path reference trajectory (dashed-orange) and vehicle trajectory (blue) of (a) one module, and (b) four assembled modules.

$K_{D,y} = K_{D,z} = 0.003$, $K_{P1,\text{alt}} = 1, K_{P2,\text{alt}} = 4, K_{I,\text{alt}} = 2$ and $K_{D,\text{alt}} = 0$. Control inputs are mapped to the corresponding propellers' (see the relation in (1)).

In the first example, we examine roll and pitch angles control. We set $\mathbf{Q}_{\text{sp}} = [1\ 0\ 0\ 0]^\top$, i.e. hover state. However, we set initial orientation of $[0.03\ 0.03\ 0]^\top$, represented in Euler angles (rad). We also want to maintain altitude and initialize the altitude at 2m and set $z_d = 2\text{m}$. We consider starting from rest. You can see the result in Figure 5. The system achieves its objective in all cases; the number of modules has some effect on performance but not significant.

Next, we examine altitude control. We set both setpoint and initial orientation $[1\ 0\ 0\ 0]^\top$ in quaternion representation or $[0\ \ 0\ \ 0]^\top$ represented in Euler angles (rad). We also consider starting from rest. We set both initial altitude to 2m, and setpoint altitude to 5m. You can see the result in Figure 6. The system achieves its objective in all cases, with negligible effect of the number of modules on the altitude control performance.

VI. Experimental Results

In this section we investigate the behavior of the used controller in the TetraQuad experimentally. The flight experiment assessed one module, and four assembled modules of the TetraQuad. The vehicles are tested by flying them to follow a circular path trajectory. The test flights have been done in an indoor flying arena, where the position of the vehicle is captured using an OptiTrack[2] motion capture system; it is fed to the flight controller, Pixhawk4 [3], of each module as position measurements of the vehicle; the IMU of the flight controller provides the orientation and angular velocity measurements. In addition, the controller parameters used are the same values used in Section V. Additionally a position controller, that sends roll and pitch set points to the attitude controller, is utilized. This position controller consists of two cascaded PID controllers [18]. The experiment is conducted at the RISC Lab at KAUST. We collect needed measurements using ROS [4] nodes and MAVROS [5] package via Wi-Fi. For safety purposes, during the flight tests the vehicle is tethered by a cable.

The individual module is tested to fly along a circular path of 0.8 meter radius, with an altitude of 1.0 meter, where the average speed is $0.6m/s$. The four-module assembly is tested to follow a 1.0 meter radius circular path at 1.0 meter altitude, with an average speed of $0.5m/s$. Figure 7 shows a picture of the TetraQuad single module and assembled modules during the experimental test. In addition, a video of the experiment is available in the paper's accompanying video file, and at `https://youtu.be/0ytmae9OLe8`.

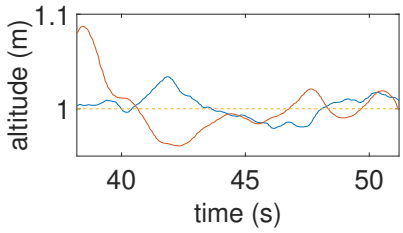

Fig. 9. Altitude comparison of flight test of one module (blue), and four assembled modules (orange) with set-point (dashed-yellow)

It can be concluded that the assembled system is able to follow the circular path trajectory in stable manner. Although the assembled system shows more oscillations than the single module, the use of the proposed controller, which emphasizes the modularity of the system, followed the mission as desired. The circular path following of both one module and four assembled modules is shown in Figure 8. Figure 9 is a comparison between a single module and four assembled modules for the altitude trajectory. Although the four assembled modules have more oscillations, the altitude oscillations have a minor error, less than 10 percent. These results indicate the controllability of the modular tetrahedral fractal aerial vehicle, TetraQuad, and its assemblies.

VII. Conclusion and Future Work

This paper discussed the TetraQuad, a new design of fractal tetrahedron aerial robot. We illustrated the design of the vehicle and its ability to fly in a stable manner. We have also discussed the modular controller strategy to fly multiple assembled vehicles, and showed the eligibility of using this proposed controller to fly tetrahedral assembly of vehicles. The verification of our system included simulation results as well as experimental validation by a number of flight tests of assembled modules.

A future work can include a more extensive analysis of the controller of this vehicle to improve its performance. Moreover we are currently working on experimentally validating our system when we have sixteen modules. In addition, we want to investigate the optimization of the power consumption of the assembled vehicles.

[2]https://optitrack.com/
[3]https://docs.px4.io/main/en/flight_controller/pixhawk4.html
[4]https://wiki.ros.org/
[5]https://github.com/mavlink/mavros

REFERENCES

[1] H. Ahmadzadeh, E. Masehian, and M. Asadpour, "Modular robotic systems: Characteristics and applications," *Journal of Intelligent & Robotic Systems*, vol. 81, no. 3, pp. 317–357, 2016.

[2] C. H. Belke and J. Paik, "Mori: a modular origami robot," *IEEE/ASME Transactions on Mechatronics*, vol. 22, no. 5, pp. 2153–2164, 2017.

[3] D. Bie, G. Liu, Y. Zhang, J. Zhao, and Y. Zhu, "Modeling the fractal development of modular robots," *Advances in Mechanical Engineering*, vol. 9, no. 3, p. 1687814017695692, 2017.

[4] D. Brescianini, M. Hehn, and R. D'Andrea, "Nonlinear quadrocopter attitude control: Technical report," ETH Zurich, Tech. Rep., 2013.

[5] S. J. Carlson, P. Arora, and C. Papachristos, "A multi-vtol modular aspect ratio reconfigurable aerial robot," in *2022 International Conference on Robotics and Automation (ICRA)*. IEEE, 2022, pp. 8–15.

[6] M. J. Duffy and A. Samaritano, "The lift! project-modular, electric vertical lift system with ground power tether," in *33rd AIAA Applied Aerodynamics Conference*, 2015, p. 3013.

[7] J. Epps, K. Garanger, and E. Feron, "Wake interactions of a tetrahedron quadcopter," in *2020 International Conference on Unmanned Aircraft Systems (ICUAS)*. IEEE, 2020, pp. 1852–1859.

[8] E. Fresk and G. Nikolakopoulos, "Full quaternion based attitude control for a quadrotor," in *2013 European control conference (ECC)*. IEEE, 2013, pp. 3864–3869.

[9] K. Garanger, "Versatile and structurally efficient aerial systems assembled from polyhedral rotorcraft modules," Ph.D. dissertation, Georgia Institute of Technology, 2022.

[10] K. Garanger, J. Epps, and E. Feron, "Modeling and experimental validation of a fractal tetrahedron uas assembly," in *2020 IEEE Aerospace Conference*. IEEE, 2020, pp. 1–11.

[11] K. Kawasaki, Y. Motegi, M. Zhao, K. Okada, and M. Inaba, "Dual connected bi-copter with new wall trace locomotion feasibility that can fly at arbitrary tilt angle," in *2015 IEEE/RSJ International Conference on Intelligent Robots and Systems (IROS)*. IEEE, 2015, pp. 524–531.

[12] A. Lyder, R. F. M. Garcia, and K. Stoy, "Mechanical design of odin, an extendable heterogeneous deformable modular robot," in *2008 IEEE/RSJ International Conference on Intelligent Robots and Systems*. Ieee, 2008, pp. 883–888.

[13] A. Martins, J. Almeida, C. Almeida, R. Pereira, D. Sytnyk, E. Soares, B. Matias, T. Pereira, and E. Silva, "Mara-a modular underwater robot for confined spaces exploration," in *Global Oceans 2020: Singapore–US Gulf Coast*. IEEE, 2020, pp. 1–6.

[14] B. Mu and P. Chirarattananon, "Universal flying objects: Modular multirotor system for flight of rigid objects," *IEEE Transactions on Robotics*, vol. 36, no. 2, pp. 458–471, 2019.

[15] R. Naldi, F. Forte, A. Serrani, and L. Marconi, "Modeling and control of a class of modular aerial robots combining under actuated and fully actuated behavior," *IEEE Transactions on Control Systems Technology*, vol. 23, no. 5, pp. 1869–1885, 2015.

[16] E. H. Østergaard, K. Kassow, R. Beck, and H. H. Lund, "Design of the atron lattice-based self-reconfigurable robot," *Autonomous Robots*, vol. 21, no. 2, pp. 165–183, 2006.

[17] R. Oung and R. D'Andrea, "The distributed flight array," *Mechatronics*, vol. 21, no. 6, pp. 908–917, 2011.

[18] PX4autopilot, "Controller diagrams | px4 user guide," 8 2022, http://docs.px4.io/main/en/flight_stack/controller_diagrams.html.

[19] D. Saldaña, B. Gabrich, G. Li, M. Yim, and V. Kumar, "Modquad: The flying modular structure that self-assembles in midair," in *2018 IEEE International Conference on Robotics and Automation (ICRA)*. IEEE, 2018, pp. 691–698.

[20] D. Saldaña, P. M. Gupta, and V. Kumar, "Design and control of aerial modules for inflight self-disassembly," *IEEE Robotics and Automation Letters*, vol. 4, no. 4, pp. 3410–3417, 2019.

[21] M. T. Shahab, O. Wali, and E. M. Feron, "Automatic identification of a modular unmanned aerial system (uas) with experimental verification," in *AIAA SCITECH 2023 Forum*, 2023, p. 2160.

[22] J. Xu, D. S. D'Antonio, and D. Saldaña, "H-modquad: Modular multirotors with 4, 5, and 6 controllable dof," in *2021 IEEE International Conference on Robotics and Automation (ICRA)*. IEEE, 2021, pp. 190–196.

[23] M. Yim, "Modular self-reconfigurable robot systems: Challenges and opportunities for the future," *IEEE Robotics Automat. Mag.*, vol. 10, pp. 2–11, 2007.

[24] M. Zhao, T. Anzai, F. Shi, X. Chen, K. Okada, and M. Inaba, "Design, modeling, and control of an aerial robot dragon: A dual-rotor-embedded multilink robot with the ability of multi-degree-of-freedom aerial transformation," *IEEE Robotics and Automation Letters*, vol. 3, no. 2, pp. 1176–1183, 2018.